

# Ultra-low background measurements in a large volume underground detector.

G. Alimonti<sup>g</sup>, G. Anghloher<sup>d</sup>, C. Arpesella<sup>a</sup>, M. Balata<sup>a</sup>, G. Bellini<sup>g\*</sup>, J. Benziger<sup>l</sup>, S. Bonetti<sup>g</sup>, L. Cadonati<sup>a</sup>, F.P. Calaprice<sup>k</sup>, G. Cecchet<sup>i</sup>, M. Chen<sup>k</sup>, N. Darnton<sup>k</sup>, A. de Bari<sup>i</sup>, M. Deutsch<sup>b</sup>, F. Elisei<sup>j</sup>, F. von Feilitzsch<sup>d</sup>, C. Galbiati<sup>g</sup>, F. Gatti<sup>e</sup>, M.G. Giammarchi<sup>g</sup>, T. Goldbrunner<sup>d</sup>, A. Golubchikov<sup>c</sup>, A. Goretti<sup>g</sup>, T. Hagner<sup>d</sup>, F.X. Hartmann<sup>g</sup>, R. von Hentig<sup>d</sup>, G. Heusser<sup>f</sup>, A. Ianni<sup>g</sup>, J. Jochum<sup>d</sup>, M. Johnson<sup>l</sup>, M. Laubenstein<sup>a</sup>, P. Lombardi<sup>g</sup>, S. Magni<sup>g</sup>, S. Malvezzi<sup>g</sup>, I. Manno<sup>g</sup>, G. Manuzio<sup>e</sup>, F. Masetti<sup>j</sup>, U. Mazzucato<sup>j</sup>, E. Meroni<sup>g</sup>, M. Neff<sup>d</sup>, A. Nostro<sup>e</sup>, L. Oberauer<sup>d</sup>, A. Perotti<sup>i</sup>, A. Preda<sup>g</sup>, R.S. Raghavan<sup>h</sup>, G. Ranucci<sup>g</sup>, E. Resconi<sup>g</sup>, M. Ruscitti<sup>e</sup>, R. Scardaoni<sup>g</sup>, S. Schönert<sup>d</sup>, O. Smirnov<sup>c</sup>, R. Tartaglia<sup>a</sup>, G. Testera<sup>e</sup>, P. Ullucci<sup>g</sup>, R.B. Vogelaar<sup>k</sup>, S. Vitale<sup>e</sup>, M. Wojcik<sup>f</sup>, O. Zaimidoroga<sup>c</sup>.

## BOREXINO COLLABORATION

- a) Laboratori Nazionali del Gran Sasso - Assergi (Aq) - Italy
- b) Massachusetts Inst. of Technology - Cambridge MA - USA
- c) Joint. Inst. for Nuclear Research - Dubna - Russia
- d) Technical Univ. Munich - Garching - Germany
- e) Physics Dept. of the University and INFN - Genova - Italy
- f) Max-Planck-Institute f. Kernphysik - Heidelberg - Germany
- g) Physics Dept. of the University and INFN - Milano - Italy
- h) Bell Laboratories - Murray Hill NJ- USA
- i) Physics Dept. of the University and INFN - Pavia - Italy
- j) Physics Dept. of the University and INFN - Perugia - Italy
- k) Physics Dept. Princeton University - Princeton NJ - USA
- l) Engineering Dept. Princeton University - Princeton NJ - USA

## Abstract

A large volume (4.8 m<sup>3</sup>) liquid scintillator detector has been running in Hall C of the Gran Sasso Underground Laboratory since February 1995. This detector is called the "Counting Test Facility" (CTF).

The main goal of the detector facility is the measurement of ultralow background levels in scintillators and the development of processes able to purify them at this level. The detector has been designed to have exceptional sensitivity using a variety of methods to identify backgrounds.

With the CTF, records were achieved in the domain of low background large volume detectors. Limits of  $3.5 \pm 1.3 \times 10^{-16}$  g/g and  $4.4_{-1.2}^{+1.5} \times 10^{-16}$  g/g for the <sup>238</sup>U and <sup>232</sup>Th daughters, respectively, and  $1.85 \pm 0.13 \pm 0.01 \times 10^{-18}$  for the isotopic abundance of <sup>14</sup>C relative to <sup>12</sup>C were obtained.

These results are very encouraging and point towards the feasibility of low energy, real time scintillation detectors for solar neutrinos, such as Borexino.

PACS number.: 10.00, 29.70

Keywords: Solar neutrino; Low radioactivity; Low background experiments.

\*Corresponding author: Physics Department and INFN, Via Celoria, 16 - 20133 Milano - Italy  
- e-mail: Gianpaolo.Bellini@Mi.INFN.IT, Phone n. 39-2-2392370, fax n. 39-2-2392617.

# 1 Introduction

Underground experiments designed to identify rare events, including solar neutrino experiments, searches for dark matter, studies of double beta decays and searches for proton decay, need very low background. The background problems are particularly hard when the detection energy threshold falls within the energy range of natural radioactivity. The difficulty is not only to reach the required radiopurity levels, but also to have a detector able to measure the counting rate at that level. (Recall that the sensitivity of a plasma source mass spectrometer is hard to push below  $\sim 10^{-12}$ g/g.)

The “Counting Test Facility” (CTF) detector was constructed to serve as a bench mark for underground experiments based on liquid scintillators and to provide a high sensitivity spectrometer to measure very low level backgrounds. It has been running in Hall C of the Gran Sasso Laboratory (LNGS) since February 1995.

The detector is designed to allow one to:

- check construction material for very low radio-activity;
- check purification methods for bulk shielding and detecting materials, such as water and aromatic-based liquid scintillators;
- determine the optical properties of liquid scintillators;
- implement cleaning methods during the construction and the installation of the detector and of the auxiliary plants;
- develop methods of analysis able to disentangle different classes of events.

The CTF activities addressed the development of techniques which will be applied to Borexino — a real time experiment designed to study low energy solar neutrinos. The Borexino detector has a design similar to the CTF, but scaled up from 4.8 to 300 tons of scintillator, and 100 to 2000 PMT’s and more shielding [1]. In addition, some technical aspects of the detector will be different than in the CTF. The radiopurity demands of Borexino are very severe requiring that the tests carried out with the CTF be pushed to the limit of their sensitivity.

## 2 The detector

The CTF detector is briefly reviewed here. A full description and a complete discussion of its characteristics can be found in ref. [2].

The CTF detector relies on a graded shield concept where each layer of shielding protects against penetrating activity from outer layers. The final shielding is provided by the active part of the detector itself through use of position reconstruction which allows the definition of a fiducial volume. In principle the only remaining activity is the intrinsic activity of the scintillator itself. The scale of the C.T.F prevented realization of this ideal limit, but even so, the self-shielding nature of the design is clearly manifested in the data presented below.

The set up (Figs.1, 2) consists of an external cylindrical water tank, 11 m in diameter and 10 m high, which houses a high sensitivity spectrometer. Within the tank 100 PMT’s (with light concentrators) are fixed to a 7m diameter support structure and collect the light produced in 4.8 m<sup>3</sup> of liquid scintillator contained within a 2.1 m diameter inner vessel.

Highly purified water from a purification plant provides shielding from external radio-emanations coming from the rocks, the tank steel and its protective coating, the PMT’s, etc. Since the inner vessel is located below the midpoint of the water tank, a 15 cm thick steel plate was installed below the tank to compensate for the reduced vertical shielding on that side.

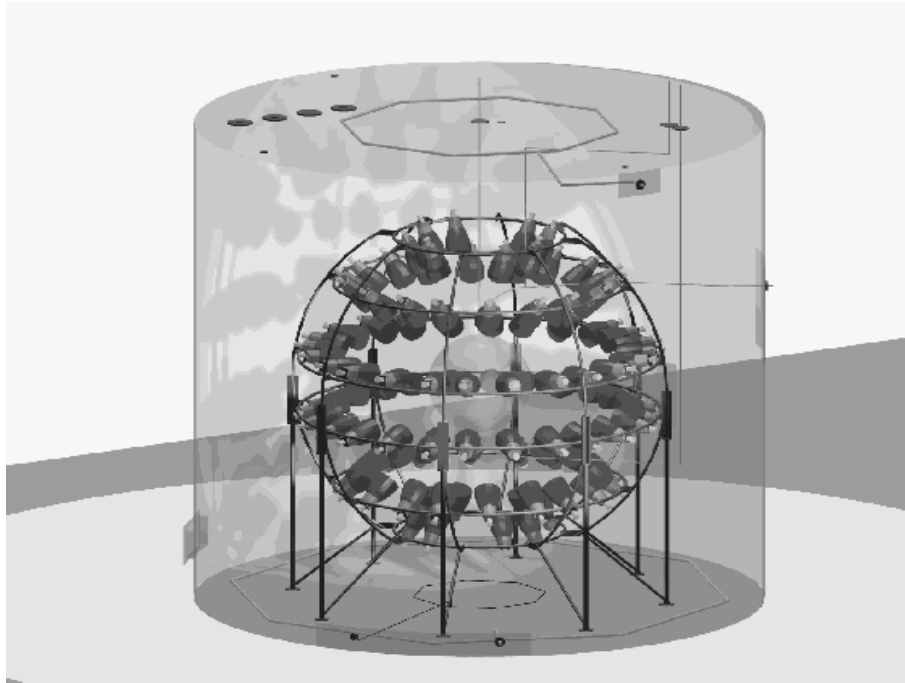


Figure 1: Sketch of the Counting Test Facility.

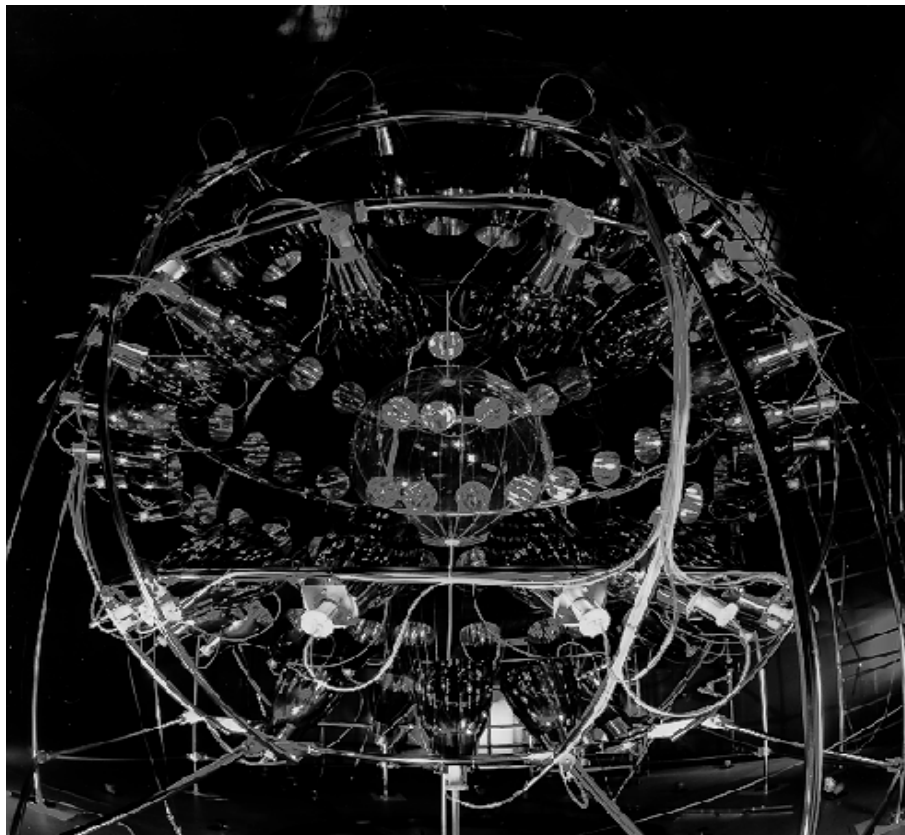


Figure 2: Photograph of the detector within the water tank.

The scintillator is handled by a liquid handling plant which interfaces between the inner vessel and a purification plant capable of: N<sub>2</sub> sparging, water extraction, and distillation.

Special care was devoted to the selection of construction materials and addressed such issues as low radioactivity, resistance to the aggressivity of very pure water and low permeability to Rn. (The air in Hall C has a Rn concentration of  $\sim 40\text{-}100$  Bq/m<sup>3</sup>.) In addition the surface finish of the plants was brought to electronics industry standards to assure the highest level of cleanliness.

## 2.1 The detector components

The external tank is made from carbon steel and coated on the inside with Permatex, an epoxy resin. The tank is coupled to a class 100 - 1000 clean room used to clean parts installed within the tank. During installation procedures the air in the tank was also filtered to maintain it at a class of a few thousand. After filling with water, a N<sub>2</sub> blanket of 10-15 mbar was maintained at the top of the tank to guard against possible leaks of external air through the flanges installed on the roof.

The PMT's are 8" Thorn EMI 9351 [3] tubes characterized by: high quantum efficiency (26% at 420 nm), limited transit time spread ( $\sigma = 1$  ns, important for a good spatial reconstruction of events), good pulse height resolution for single photoelectron pulses (Peak/Valley=2.5), low dark noise rate (0.5 kHz), low after pulse probability (2.5% - important for  $\alpha - \beta$  discrimination), and a gain of  $10^7$ . The bulbs are made out of low radioactivity Schott 8246 glass which has about 10 times less radioactivity than normal glasses. The PMT's are fitted with light concentrators 57 cm long and which have a 50 cm diameter aperture. The combination gives a 20% optical coverage for the CTF.

The scintillator is a binary solution obtained by dissolving 1.5 g/ $\ell$  of a scintillating solute, PPO(2,5-Diphenyloxazol) in pseudocumene (1,2,4-Trimethylbenzene). The fluorescence peak emission is at 365 nm, well matched to the spectral response of the phototubes. The yield of emitted photons is about 10000 per MeV of energy deposited (see ref. [4]).

For each event the charge and timing of hit phototubes is recorded. To avoid missing fast time correlated events, each processing channel is doubled by an auxiliary channel to record all other events coming within a time window of 8 ms after the first event. The time delay is determined to a precision of 1 ns. For longer correlation times, the internal clock of the computer is used (with a resolution of  $\sim 0.1$ s). The PMT analog signals are also summed and time integrated over the total pulse and the pulse tail, whose ratio can be used to discriminate between  $\alpha$  and  $\beta$  signals (see paragraph 3.4).

The scintillator containment vessel, called the Inner Vessel, is an unsegmented vessel, 2.1 m in diameter, and constructed from a membrane of amorphous nylon, 500  $\mu\text{m}$  thick, cut into "orange peels" and solvent bonded together. The optical clarity is very good at 350-500 nm and its radio-impurity levels are only  $10^{-12}$ g/g for U, Th and  $10^{-9}$  g/g for K. It was fabricated in a class 100 clean room. The vessel is installed at the center of the PMT system and is held against an upward buoyant force by 32 nylon strings. The stress of each line is continuously monitored by strain gauges.

## 2.2 Auxiliary plants

Three auxiliary plants handle the fluids. They are the water plant, the liquid handling plant, and the purification plant.

The water plant purifies the water used to fill the external tank ( $\sim 1000$  tons of water). It consists of two parts: the production line and the main circulation loop. The production line includes reverse osmosis units, a continuous deionization unit, an ultra-filtration system and a N<sub>2</sub> stripping column to remove radon. The main circulation loop recirculates the water from

Table 1: *The  $^{222}\text{Rn}$  daughters. For the  $\alpha$  emitters, the quenched energy values are also reported.*

Nuclides	Decay products	Energy (MeV)	Alpha quenched energy (keV)	Lifetime
$^{222}\text{Rn}$	$\alpha$	5.49	410	5.48 d
$^{218}\text{Po}$	$\alpha$	6.02	483	4.40 min
$^{214}\text{Pb}$	$\beta + \gamma$	1.03		38.7 min
$^{214}\text{Bi}$	$\beta + \gamma$	3.20		28.4 min
$^{214}\text{Po}$	$\alpha$	7.69	751	236 $\mu\text{s}$
$^{210}\text{Pb}$	$\beta + \gamma$	0.06		32.2 y
$^{210}\text{Bi}$	$\beta$	1.16		7.23 d
$^{210}\text{Po}$	$\alpha$	5.30	395	200 d

the water tank and restores the water purity through a de-ionizer cartridge, a  $0.1 \mu\text{m}$  filter and a  $\text{N}_2$  stripping column. The radiopurity levels of the shielding water produced by this plant are: U, Th  $\simeq 10^{-14}$  g/g;  $\text{K}_{\text{nat}} \simeq 10^{-10}$  g/g;  $\text{Rn} < 5 \mu\text{Bq}/\ell$  [5].

The fluid handling system provides for the filling and emptying of the nylon inner vessel with scintillator. It also serves several other functions including filling the inner vessel with: nitrogen during installation; water during the mechanical testing stages and cleaning; and water to displace the scintillator.

The purification system is used to purify the scintillator by recirculating it from the inner vessel. The system is composed of a Rn stripping tower, a water extraction unit, and a vacuum distillation unit.

The system is constructed with electro-polished stainless steel components (electronics grade) and features high level filtering for particulate removal. During operation the scintillator was taken from the Inner Vessel, processed through the plant and then returned in a continuous manner. As a consequence the maximum purification factor expected per cycle is  $1/e$ , assuming complete mixing.

The cleanliness requirements for the CTF are very severe, not only during the preparation of the various parts of the apparatus, but also during the installation phase. Dust and particulates are particularly dangerous so filters were installed in each plant to prevent their entry (and also the entry of any bacteria.)

### 3 Technical achievements of the CTF

Event parameters measured in the CTF include:

- the total charge collected by the PMT's, which gives a calorimetric measurement of the event energy;
- the PMT timing, used to reconstruct the event in space;
- the pulse shape of each event to discriminate between  $\alpha$ 's, electrons and other classes of events;
- the time elapsed between sequential events — provided by the auxiliary channels of the read out electronics. (This measurement was useful to tag time-correlated events produced by correlated decays in the radioactive families.)

Accurate input parameters for the reconstruction code were obtained with radioactive sources. The sources consisted of quartz vials filled with Rn spiked scintillator. These sources

were introduced into the I.V. and moved within it by means of a mechanical arm manipulated from the top of the tank. Measurements were done with the source in various positions within the vessel as well as on the vessel walls.

The scintillator decay mechanism and light propagation (including absorption, reemission and light scatter) were also studied by using a modified Rn source which had the vial completely darkened except for a small window to obtain directionality for the emitted light.

### 3.1 Energy calibration and photo-electron yield

The energy calibration was carried out by analyzing data collected just after filling the I.V. with the scintillator (which had accidentally been exposed to few liters of air, thus raising its Rn level).

The sequence  $^{214}\text{Bi}(\beta)$ - $^{214}\text{Po}(\alpha)$ , daughters of  $^{222}\text{Rn}$ , can be tagged very efficiently by identifying the  $^{214}\text{Po}$   $\alpha$  and then looking for its parent  $^{214}\text{Bi}$   $\beta$  in a coincidence time window. Recall that the alpha signals are quenched by a factor ranging from  $\sim 13$  to  $\sim 10$  (see Table 1) as the energy increases (these factors were measured off-line). The well defined  $\alpha$  peak of  $^{214}\text{Po}$  was used as a reference for the energy calibration. The energy resolution, evaluated from the width of the  $^{214}\text{Po}$  peak, is  $\sim 9\%$  ( $1\sigma$ ) and is expected to scale with energy as  $1/\sqrt{N}$  ( $N$ =number of photoelectrons).

This calibration has been checked using the Rn source described above and fluctuations versus source position of up to 10% were observed. This phenomenon, which occurs especially when the source is positioned very close to the vessel walls, is attributed to optical effects arising from the mismatched index of refraction between the water and scintillator. This mismatch gives rise to refraction and light trapping and is exacerbated by the tessellated shape of the inner vessel.

An energy linearity check was obtained via the above calibration line and the  $\alpha$  decays of  $^{222}\text{Rn}$  and  $^{218}\text{Po}$ , at 5.49 and 6.02 MeV, respectively (quenched to  $410\pm 6$  and  $483\pm 6$  keV.) Although the two signals were not well resolved, the fit confirmed linearity to within a few percent, finding  $405\pm 7$  and  $488\pm 10$  keV, respectively.

Beta signals from the decay of  $^{85}\text{Kr}$  were also studied. ( $^{85}\text{Kr}$  was initially present following the air contamination mentioned above due to its presence in air at the level of  $\sim 1\text{Bq/m}^3$ .) It was tagged by the  $^{85}\text{Kr}(\beta)$ - $^{85}\text{Rb}(\gamma)$  correlation.  $^{85}\text{Kr}$  beta decays 0.43% of the time to a metastable level of  $^{85}\text{Rb}$  at 514 keV (173 keV end point) which then gamma decays directly to the ground state with a 1.46  $\mu\text{s}$  lifetime. Simulations show that only  $\sim 10\%$  of the 514 keV gamma showers are not fully contained within the scintillator, this effect thereby having only limited impact on the peak position. The expected peak was found within 5% of the nominal energy.

The spectrum of Rn contained in the water shielding, as measured in the Inner Vessel during the ‘‘Rn test’’ described below, also offered the possibility of a linearity check using the monochromatic gamma lines penetrating into the inner vessel. We refer in particular to the 609 keV gammas emitted by the  $^{214}\text{Bi}$  decay. The measured energy spectrum shows a clear shoulder centered within a few percent of the nominal value.

The photo-electron (p.e.) yield was evaluated using the following procedure:

- a) The number of hit channels versus the number of p.e. was evaluated via a simulation using the probability relation between these two variables. (They differ because of multiple p.e. per channel.)
- b) The same relationship is measured using the experimental data.
- c) The two plots are compared and since the distance between the pedestal and the first p.e. peak in the charge distribution of the phototubes is different from those between adjacent

multiple p.e. peaks (first and second, second and third, etc.), a linear transformation of the measured photoelectron scale is applied to make them coincide.

- d) The number of photoelectrons per MeV is measured experimentally using well identified decays and applying the transformation mentioned in c).

The best value for the photoelectron yield is  $300 \pm 30$  photoelectrons/MeV on average.

### 3.2 Decay mechanism of the scintillator and light propagation.

The scintillator decay photons travel through the scintillator itself before exiting the Inner Vessel and interact both with the PPO and the PC molecules with a cross section strongly dependent on the wavelength. For the shortest wavelengths of the PPO spectrum, the interaction with PPO dominates while, for the longer wavelengths, the interaction with PC is the most important one. Photons absorbed by PPO can be re-emitted with high probability (quantum efficiency  $\simeq 0.8$ ) producing a new photon with a new  $\lambda$  value that can itself be absorbed and re-emitted. This sequence stops when the new wavelength is long enough to have a negligible interaction probability with PPO.

The interaction of photons with the PC solvent of a scintillator mixture is mainly elastic scattering for  $\lambda \geq 380$  nm (changing the direction of flight) and absorption-reemission for smaller wavelengths. As a result only a few number of photons are really lost in a spherical detector like the CTF (in contrast to detectors having a small acceptance angle where both elastic scattering processes and absorption-reemission lead to a loss of detectable photons.) The elastic scattering affects only the time distribution of the photons collected on the various PMT's. In other words, beam attenuation measurements made in the laboratory may not reflect the attenuation parameters needed for  $4\pi$  acceptance detectors.

The importance of PPO absorption and reemission was suggested by laboratory measurements and using the CTF it was possible to quantitative the effect through dedicated runs with a "window source." The number of photons reaching the PMT's on the optically occluded side and their time distribution were measured and compared with a Monte Carlo simulation including both the re-emission process from PPO and the elastic scattering from PC.

The simulation gives 46-56% of the original light detected directly, 22% absorbed and re-emitted and 12-14% lost. If we neglect this last fraction, the simulation predicts that 45-48% of the detected light should be absorbed and re-emitted, in reasonable agreement with the 44% obtained from the experimental test.

The principle scintillator decay time of  $\sim 3.5$  ns, without absorption-reemission, was obtained in small scale laboratory experiments. In contrast, the decay curve obtained with an isotropic source in the center of the CTF features a longer decay time of (4.5-5.0 ns) as expected. [see also ref. 4].

### 3.3 Spatial reconstruction and resolution

The space-time coordinates of the events are calculated from the PMT signals using the maximum likelihood method.

The arrival time  $t_a$  of each photon is given by:

$$t_a = t_0 + t_d + t_f + t_j \quad (1)$$

where  $t_0$  is the trigger time of the scintillator,  $t_d$  is the scintillator decay time,  $t_f$  is the photon time of flight and  $t_j$  is the PMT transit time. The "probability density function (pdf)" is then defined as the Laplace convolution of the probability density functions for  $t_d$  and  $t_j$ . It was simulated first and then tuned using the data collected with the Rn source. For each PMT only

the arrival time of the first photoelectron is recorded. However, the probability of having more than one p.e. per PMT increases with the energy giving the p.d.f. an energy dependence.

The trajectory of the single photon is not unambiguously determined by the start and the stop points: corrections to Fermat’s law arise from light scattering, reflections, refraction, etc.. These corrections were simulated by defining an “effective refractive index ( $n_{eff}$ )”, which was obtained by minimizing the differences between the times of flight obtained from the nominal positions of the Rn source and the reconstructed ones. Hence the time of flight  $t_f$  is defined as:

$$t_f = \frac{d_0 \times n_{eff}}{c} \quad (2)$$

where  $d_0$  is the distance between the photon production point and the PMT.

Once  $d_0$  is calculated, it is possible to evaluate  $t_d + t_j$ :

$$t_d + t_j = t_a - t_0 - \frac{d_0 \times n_{eff}}{c} \quad (3)$$

The maximum likelihood function L is defined as:

$$L(t_0, x_0, y_0, z_0) = \prod_{firedPMT's} pdf(t_d + t_j) \quad (4)$$

and the coordinates which maximize L are taken as the reconstructed coordinates.

The position resolution of the reconstruction code was checked using the Rn source at the energy of the  $^{214}\text{Po}$   $\alpha$ 's and in the energy range of the  $^{214}\text{Bi}$   $\beta$ 's. In Table 2 the x-y resolution is shown (the vial used for these particular sources was extended in the z-direction).

In Fig. 3 the nominal position of the Rn source is compared with the reconstructed one. The agreement is very good, especially in regions not very close to the vessel walls.

Another method taking into account exactly the index mismatching is still under development.

	E (keV)	$\sigma_{x,y}$ (cm)
$^{214}\text{Bi}$	150-250	$25.7 \pm 1.0$
”	250-350	$15.4 \pm 0.55$
”	350-450	$15.3 \pm 0.53$
”	450-550	$13.5 \pm 0.43$
”	550-650	$12.6 \pm 0.38$
”	650-750	$12.1 \pm 0.37$
”	750-850	$11.5 \pm 0.31$
”	850-950	$10.4 \pm 0.29$
”	950-1250	$10.1 \pm 0.17$
”	1250-1550	$9.8 \pm 0.6$
$^{214}\text{Po}$	751	$12.3 \pm 0.04$

Table 2:

### 3.4 $\alpha/\beta$ discrimination

The excitation of the scintillator depends on many factors including the energy loss density — a larger  $dE/dx$  enhances the slow component of the decay curve.



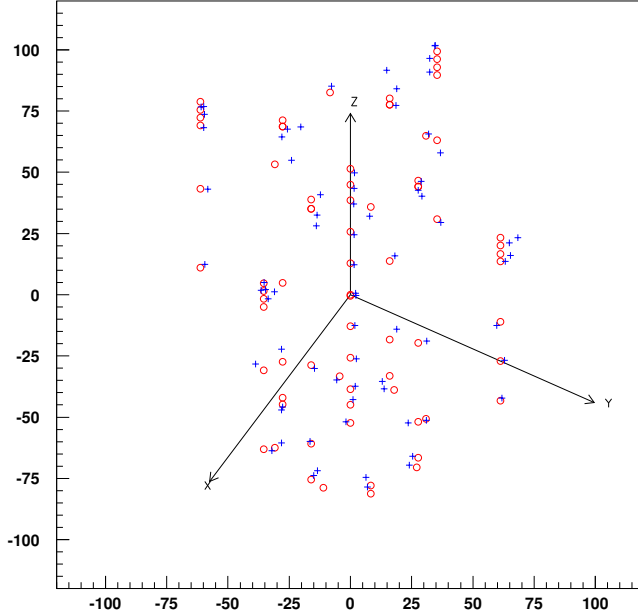


Figure 3: Comparison between the nominal positions of the Rn source (empty circles) and the reconstructed ones (small crosses).

The pulse shape for  $\alpha$ 's and  $\beta$ 's was measured for the scintillator mixture used in the CTF and different slopes for  $\alpha$  and  $\beta$  are clearly present (see Fig. 4). This characteristic was exploited to select  $\beta$ 's from  $\alpha$ 's by comparing the integrated area below the whole pulse with that below the tail only.

In the CTF the analog signals from all the PMT's were summed and the total charge found by integrating the signal over the range 0—500 ns, while the tail charge was found by integrating over the range 48-500 ns. The ratio of these two charges (tail over total) is expected to be greater for alphas than for electrons. In Fig. 5 the tail charge/total charge ratio is plotted vs energy. The  $\alpha$ 's from  $^{214}\text{Po}$  (high energy) and from  $^{222}\text{Rn}$  and  $^{218}\text{Po}$  (low energy) can be easily separated from the continuous beta spectrum of  $^{214}\text{Bi}$ . The tail/total charge ratio varies with the radial position of the event due to time of flight differences. To compensate for this,  $\alpha/\beta$  discrimination parameters were adjusted as a function of radius.

Applying these procedures to the central part of the detector ( $r < 60$  cm) we observed an efficiency for alpha identification of  $\sim 97\%$  at 751 keV ( $^{214}\text{Po}$ ) with an associated  $\beta$  misidentification of  $\sim 2.5\%$ . At lower energies (300-600 keV) the  $\alpha$  identification efficiency ranges from 90 to 97% with an associated  $\beta$  misidentification of 10%.

## 4 Sensitivity of the detector

The Counting Test Facility is one of the most sensitive large volume detectors in the world. Presently, without any selection based upon spatial reconstruction, the total counting rate of the detector between 250 KeV and 2.5 MeV is about  $0.03 \text{ counts kg}^{-1} \text{ keV}^{-1} \text{ yr}^{-1}$ . We present here the minimum contamination levels of  $^{14}\text{C}$  and radionuclides in the U and Th chains detectable

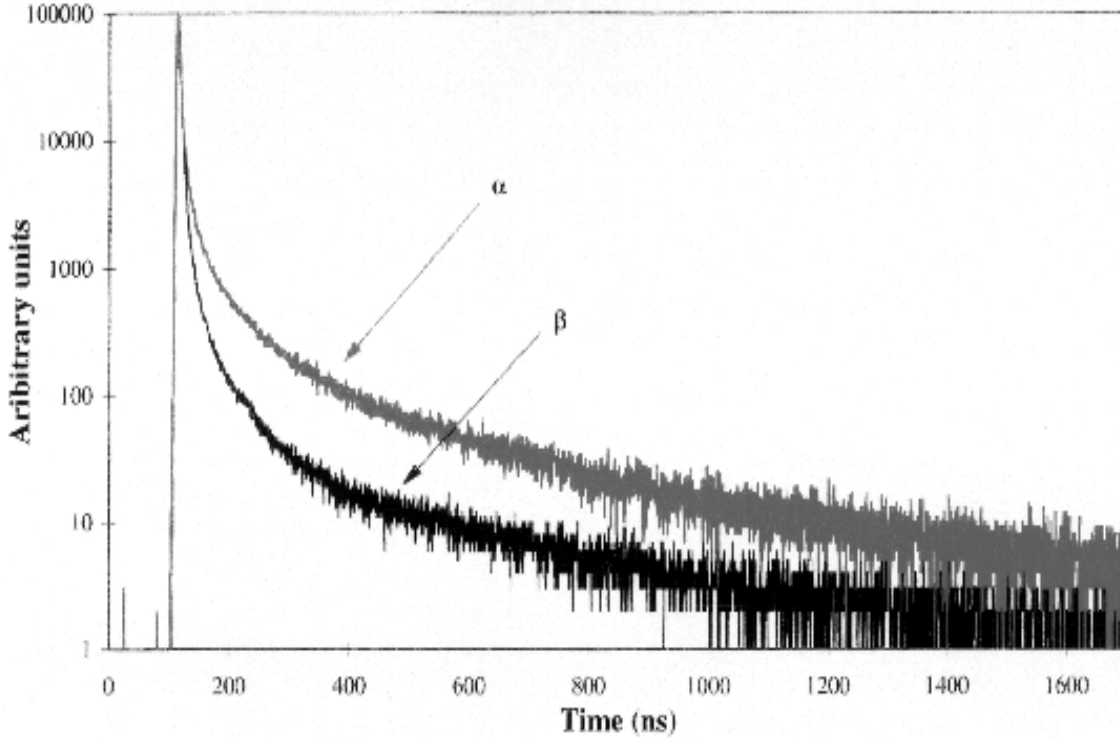


Figure 4: Scintillator pulse shapes for the detection of  $\alpha$ 's and electrons.

with the CTF after one year of data taking.

$^{14}\text{C}$  can be determined by measuring the total counting rate between 70 and 150 keV and fitting this region with the  $^{14}\text{C}$  beta spectrum calculated via Monte Carlo simulations, taking into account possible backgrounds due to contaminations within the scintillator and the external background. These backgrounds are the limiting factor in measuring the  $^{14}\text{C}$  with the consequence that the lowest  $^{14}\text{C}/^{12}\text{C}$  ratio which can be measured in the CTF is  $\sim 10^{-19}$  ( $3\sigma$  confidence level).

The Th and U abundances can be inferred by assuming secular equilibrium in their decay chains and then measuring correlated events belonging to the two radioactive families. These events are measured through delayed coincidences, making use of the main and auxiliary electronic channels. High sensitivities can be achieved by studying the shortest time correlations and in this way the background due to random coincidences is minimized.

The most convenient coincidence for the  $^{238}\text{U}$  family is the correlated coincidence  $^{214}\text{Bi}(\beta\gamma)$  -  $^{214}\text{Po}(\alpha)$  (see Table 1) with a time delay of  $236 \mu\text{s}$ .  $^{214}\text{Bi}$  is a  $\beta + \gamma$  emitter with a spectrum which extends up to 3.27 MeV; the  $^{214}\text{Po}$  decay emits a 7.69 MeV  $\alpha$  (reduced to  $751 \pm 7$  keV by the quenching factor). Selection of the correlated candidates can be carried out via the following cuts:

- a) the energy of the events measured by the main (start) channel has to be  $>300$  keV. This cut rejects 90% of the random coincidences and accepts 97% of the  $^{214}\text{Bi}$  decays;
- b) the energy in the auxiliary (stop) channel has to be within  $2\sigma$  of the  $^{214}\text{Po}$  decay alpha peak. This cut helps reject random coincidences and accepts (98%) of the true coincidences;
- c) the coincidence time has to be between 20 and  $500 \mu\text{s}$ . The lower cut removes the PMT

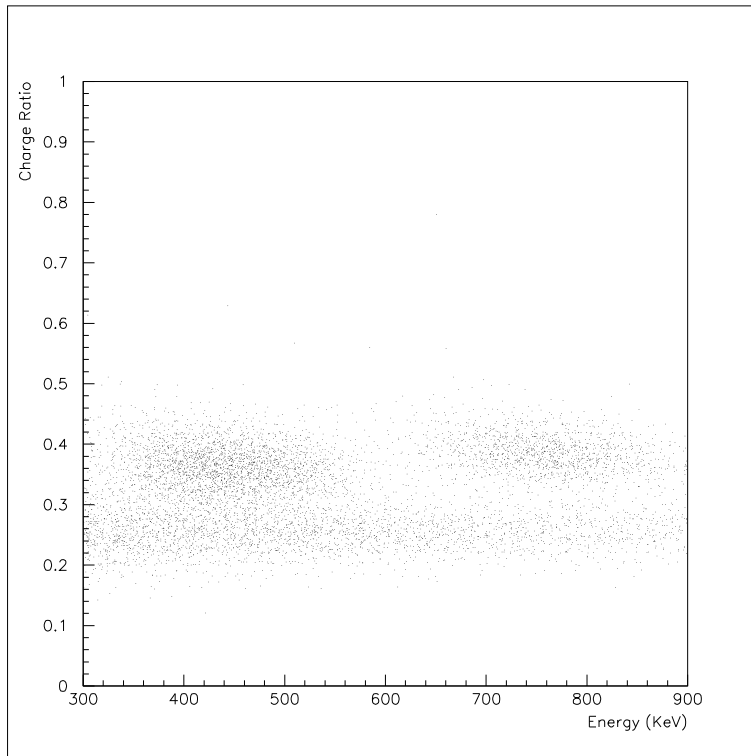


Figure 5: Results of the  $\alpha/\beta$  discrimination. The  $\alpha$ 's from  $^{214}\text{Po}$  (high energy) and from  $^{222}\text{Rn}$  and  $^{218}\text{Po}$  (low energy) can be easily separated from the continuous beta spectrum of  $^{214}\text{Bi}$  corresponding to a charge ratio of  $\sim 0.2-0.3$ .

after-pulses; the upper limit corresponds to two  $^{214}\text{Po}$  lifetimes. The acceptance of this time cut is 80%.

The CTF sensitivity to this coincidence is  $0.5 \pm 0.3$  coincidences  $\text{day}^{-1} \text{ton}^{-1}$  corresponding in principle to  $1.2 \pm 0.9 \times 10^{-16} \text{g(U)/g(scintillator)}$ . The actual rate we see may, however, reflect Rn from other sources diffusing into the IV rather than the intrinsic Ra in the scintillator.

Similar technique can be used for the nuclides of the Th family. In this case the correlated events  $^{212}\text{Bi} - ^{212}\text{Po}$  (see Table 3), with a time delay of 432.8 ns, are the most convenient.  $^{212}\text{Bi}$  emits  $\beta$ 's +  $\gamma$ 's with a spectrum which extends up to 2.25 MeV;  $^{212}\text{Th}$  emits  $\alpha$ 's of 8.785 MeV, quenched to 1010 keV.

The selective criteria are very similar to those applied in the  $^{238}\text{U}$  analysis. The cut in a) is the same, but in this case 10% of the  $^{212}\text{Po}$  coincidences are missed; the requirement in b) and its efficiencies are the same, while the coincidence time lies between 100 and 1000 ns (the lower limit takes into account the dead time of the read-out electronics (50 ns)); the upper one corresponds to two  $^{212}\text{Po}$  lifetimes (acceptance: 70%).

The lowest measurable limit for the Th family ( $3\sigma$ ) is  $10^{-17} \text{g/g}$  (limited by statistics).

## 5 Measurement of the background levels in the CTF

The Counting Test Facility has been taking data since February 1995. Two runs were done at the beginning, one with the inner vessel and external tank filled with  $\text{N}_2$ ; a second one with them filled with water. During March 1995 data was collected with  $1 \text{ m}^3$  of scintillator in the inner

vessel. During May-June 1995 several runs were carried out with the inner vessel completely filled ( $4.8 \text{ m}^3$ ) with scintillator (PC+PPO) whose only purification had been distillation of pseudocumene during synthesis and water extraction of the fluor. The Pseudocumene was produced by Enichem at Sarroch in Sardinia.

During July-August 1995 the scintillator was purified by  $\text{N}_2$  sparging and water extraction and in October by distillation. Data was collected continuously during these periods.

Various tests were conducted through August 1996. They included measurements using Rn sources inserted into the Inner Vessel (see sec. 3) to calibrate the detector. In addition a few  $\text{m}^3$  of water which had not been sparged with  $\text{N}_2$  were injected into the shielding water greatly increasing the Rn level in the water. This “Rn test” was to study the behavior of the external background discussed below.

The counts registered by the CTF detector are classified as “background,” because the neutrino signal is negligible. The background can have different sources: i) contamination of the scintillator itself; ii) radioactivity of the water, PMT’s and other materials used in the CTF construction, which produce gammas penetrating into the Inner Vessel; iii) decay of contaminants on the inner vessel itself; iv) cosmic-ray induced events; and v) spurious events.

In the following we define “External Background” as the counting rate due to background sources outside the I.V. and thus not connected with the scintillator and we define “Internal Background” as the counting rate due to scintillator contaminants.

It is possible that contributions to the counting rate could be due to decays of contaminants implanted on the internal surface of the I.V. walls. Rn nuclei which decay close to an uncovered nylon surface can have their daughters implanted into the material. Because of their short lifetime the first daughters do not pose a problem. The long lifetime of  $^{210}\text{Pb}$  (see Table 1), however, means that the  $^{210}\text{Pb}$ ,  $^{210}\text{Po}$  and  $^{210}\text{Bi}$  decay chain is observed for a long time.  $^{210}\text{Pb}$  emits below 100 keV, in the energy region dominated by  $^{14}\text{C}$  and so is not a problem. On the other hand the decay products of  $^{210}\text{Po}$  and  $^{210}\text{Bi}$ , which are  $\alpha$  and pure  $\beta$  emitters, are in the region of interest. The nylon of the vessel was covered almost completely during construction which occurred in a dust free but not Rn free atmosphere. During installation, however, the vessel was exposed to air whose Rn level was high. The possible contribution of the I.V. internal surfaces to the background is referred to as “Surface Background.”

The light concentrators, coupled with the PMT’s, are designed to optimize the collection of the light produced within the inner vessel. Nevertheless they are not blind to light produced in the shielding water due to the Čerenkov effect. A successful criteria for identifying these events was developed during the so called “water run”, when the Inner Vessel, as well as the external tank, was filled with water and will be explained later.

Recently, the CTF was shut down to replace the phototubes. The percentage which failed ( $> 80\%$ ) was abnormal and believed to be due to poor sealing between silicon gel and the polyethylene jacket of the cables. This problem was undoubtedly exacerbated by the presence of pseudocumene in the water which arose due to an accidental introduction of  $\sim 70\ell$  of pseudocumene into the water early in the program (and subsequently removed.) The sealing of the PMT’s has now been redesigned to resist both water and PC.

## 5.1 Identification of the events

The first step of the data analysis is the separation of valid events into those associated with Čerenkov light produced in the shielding water by cosmic rays [ $1 \text{ muon m}^{-2} \text{ hr}^{-1}$  in the Gran Sasso Laboratory] and gammas, versus events occurring in the scintillator.

Tags for Čerenkov events were obtained by analyzing the “water data”, collected when the Inner Vessel was filled with water. In Fig. 6 the spectrum of the Čerenkov radiation detected by the CTF spectrometer is shown. The low energy region of the spectrum [plotted in